JOURNAL OF GEOPHYSICAL RESEARCH, VOL. 114, C03006, doi:10.1029/2008JC004919, 2009

Satellite microwave observations of the interannual variability of snowmelt on sea ice in the Southern Ocean

Sascha Willmes,[1] Christian Haas,[2,3] Marcel Nicolaus,[4] and Jörg Bareiss[1]

Received 19 May 2008; revised 10 December 2008; accepted 6 January 2009; published 7 March 2009.

[1] Snowmelt processes on Antarctic sea ice are examined. We present a simple snowmelt indicator based on diurnal brightness temperature variations from microwave satellite data. The method is validated through extensive field data from the western Weddell Sea and lends itself to the investigation of interannual and spatial variations of the typical snowmelt on Antarctic sea ice. We use in-situ measurements of physical snow properties to show that despite the absence of strong melting, the summer period is distinct from all other seasons with enhanced diurnal variations of snow wetness. A microwave emission model reveals that repeated thawing and refreezing cause the typical microwave emissivity signatures that are found on perennial Antarctic sea ice during summer. The proposed melt indicator accounts for the characteristic phenomenological stages of snowmelt in the Southern Ocean and detects the onset of diurnal snow wetting. An algorithm is presented to map large-scale snowmelt onset based on satellite data from the period between 1988 and 2006. The results indicate strong meridional gradients of snowmelt onset with the Weddell, Amundsen, and Ross Seas showing earliest (beginning of October) and most frequent snowmelt. Moreover, a distinct interannual variability of melt onset dates and large areas of first-year ice where no diurnal freeze thawing occurs at the surface are determined.

Citation: Willmes, S., C. Haas, M. Nicolaus, and J. Bareiss (2009), Satellite microwave observations of the interannual variability of snowmelt on sea ice in the Southern Ocean, *J. Geophys. Res.*, *114*, C03006, doi:10.1029/2008JC004919.

1. Introduction

[2] The spatial and temporal variability of sea ice and its snow cover and the seasonal cycle of their physical properties are of great importance for the global surface energy budget. The high albedo and low thermal conductivity of sea ice and snow result in the reflection of solar radiation and the attenuation of the exchange of heat, mass and momentum between the ocean and the atmosphere [e.g., *Wadhams*, 2000]. The snow cover significantly enhances the role of sea ice in the global climate system because of its even higher albedo and lower thermal conductivity, while it reacts much faster to atmospheric forcing [*Hanesiak et al.*, 1999]. Snowmelt onset is of particular importance during the seasonal cycle of sea-ice surface properties. It triggers a decrease in surface albedo [*Perovich*, 1996], which causes an increased absorption of solar radiation, the occurrence of ice-albedo feedback mechanisms [*Curry et al.*, 1995] and thus changes in the surface energy balance. Furthermore, snowmelt onset is a frequently discussed proxy, to describe environmental changes in large-scale climate studies [e.g., *Anderson and Drobot*, 2001].

[3] Rapid snowmelt is frequently observed in the Arctic, leading to the disappearance of the snow cover and the formation of melt ponds during summer [e.g., *Fetterer and Untersteiner*, 1998]. In contrast, on Antarctic sea ice, snow covers generally last over the whole summer, because cold dry air masses, high wind speeds [*Andreas and Ackley*, 1982] and an accompanying low net surface heat gain [*Vihma et al.*, 2009] do not allow strong snowmelt. Therefore the contribution of evaporation to the seasonal loss of snow mass is about five times higher on Antarctic sea ice [*Nicolaus et al.*, 2006; M. Nicolaus et al., Evolution of first and second-year snow properties on sea ice in the Weddell Sea during late spring, submitted to *Journal of Geophysical Research*, 2009, hereinafter referred to as Nicolaus et al., submitted manuscript, 2009] and snow wetting occurs mostly with the course of the diurnal cycle [*Willmes et al.*, 2006; *Vihma et al.*, 2009]. Especially on perennial Antarctic sea ice, snow survives the summer season, becomes highly metamorphous [*Massom et al.*, 2001], and transforms frequently into a layer of superimposed ice at the snow-ice boundary [*Haas et al.*, 2001; *Nicolaus et al.*, 2003], which can significantly contribute to the sea-ice mass [*Eicken*, 1998; *Haas et al.*, 2001].

[4] On the basis of the seasonal cycle of microwave signatures of Arctic sea ice, *Livingstone et al.* [1987] identified three phenomenological stages of snowmelt,

[1]Department of Environmental Meteorology, University of Trier, Trier, Germany.
[2]Climate Division, Alfred-Wegener Institute for Polar and Marine Research, Bremerhaven, Germany.
[3]Now at Department of Earth and Atmospheric Sciences, University of Alberta, Edmonton, Alberta, Canada.
[4]Polar Environmental Centre, Norwegian Polar Institute, Tromsø, Norway.

0148-0227/09/2008JC004919$09.00

namely "*Early Melt, Melt Onset and Advanced Melt*". In this classification scheme *Melt Onset* denotes the seasonal stage when meltwater in the snow pack does not refreeze overnight and the surface energy budget becomes continuously positive. With respect to climate studies, *Melt Onset* thus represents an important transition in the seasonal cycle of the surface energy budget and several approaches were proposed to identify this stage from long-term passive and active microwave satellite data.

[5] *Comiso* [1983] reported a rapid seasonal increase of the microwave emissivity (ε) from Arctic sea ice that is coupled with the formation of meltwater in the snow pack [*Maslanik and Barry*, 1989]. The formation of liquid water causes an increase in the microwave brightness temperature (T_B) as observed by the *Scanning Multichannel Microwave Radiometer* (SMMR) and the *Special Sensor Microwave/Imager* (SSM/I) sensors during the transition from spring to summer. *Anderson* [1987] and *Serreze et al.* [1993] used this feature to derive snowmelt onset dates for sea ice in the Arctic. In concert with the increase of T_B, radar backscatter (σ^0) decreases. This drop was detected as an indicator for the onset of snowmelt [*Perovich et al.*, 2007; *Barber et al.*, 1998; *Winebrenner et al.*, 1994]. Advanced snowmelt investigations reconsider the potential of advanced channel combinations and methods to identify the melt onset stage from microwave satellite data for snow on sea ice [*Anderson and Crane*, 1994; *Anderson*, 1997; *Smith*, 1998; *Drobot and Anderson*, 2001a; *Belchansky et al.*, 2004a], snow on ice sheets [*Abdalati and Steffen*, 1987; *Mote and Anderson*, 1995; *Mote*, 2007] and on continental snow cover [*Koskinen et al.*, 1997]. Recent studies suggest the use of diurnal T_B variations for snowmelt monitoring on the Greenland ice sheet [*Ashcraft and Long*, 2005; *Tedesco*, 2007].

[6] Applied to long-term satellite data, these methods revealed a trend toward earlier melt onset dates and an extended snowmelt season on Arctic sea ice from 1979 to 1998 [*Drobot and Anderson*, 2001b; *Anderson and Drobot*, 2001] and from 1979 to 2001 [*Belchansky et al.*, 2004b], indicating climate change in the Arctic.

[7] As discussed above, persistent melting occurs only sporadically on sea ice in the Antarctic. In this paper, we will therefore describe a method which detects the onset of diurnal melting events, which applies rather to the Early Melt stage in the classification scheme of *Livingstone et al.* [1987].

[8] Sea ice in the Southern Ocean has been subject to only a few snowmelt studies. Characteristic for Antarctic sea ice is a generally thicker snow cover than in the Arctic [*Warren et al.*, 1999; *Massom et al.*, 2001; *Markus and Cavalieri*, 2007], the widespread formation of snow ice after flooding [*Jeffries et al.*, 1997; *Haas et al.*, 2001] and a different crystal structure with more granular ice [*Tucker et al.*, 1987; *Lange et al.*, 1989; *Comiso et al.*, 1992]. As a result of this, together with the processes in the snow outlined above, the seasonal cycles of perennial Antarctic sea-ice T_B and σ^0 are actually opposite to those in the Arctic, with T_B decreasing and σ^0 strongly rising at the beginning of summer [*Kern and Heygster*, 2001; *Haas*, 2001]. This impedes a transfer of snowmelt detection methods from the Northern Hemisphere. However, *Drinkwater and Liu* [2000] applied an algorithm that detects meltwater-induced decreases of σ^0 to identify the onset of snowmelt on Antarctic sea ice. This radiometric behaviour is mostly limited to first-year ice areas close to the marginal ice zone. Consequently, they found melt periods to be lasting only a few days long, and just before the ice actually disappeared. *Willmes et al.* [2006] investigated the role of diurnal processes for the seasonal cycle of sea-ice T_B in the Antarctic. They found that extensive diurnal freeze-thaw cycles are prevailing on perennial ice and cause a rounding and growth of snow grains. The resulting snow metamorphosis leads to a decrease of ε and causes the observed drop of T_B on Antarctic sea ice during summer.

[9] On the basis of the results of *Willmes et al.* [2006], we review in this paper the effects of changing snow properties at the beginning of summer on the microwave signatures of Antarctic sea ice. Hereafter, we introduce a new algorithm for the detection of snowmelt onset on sea ice in the Antarctic.

[10] The interpretation of microwave signatures is based on an extensive field study, where detailed in-situ measurements of various relevant snow properties were performed. Results of the field measurements are used to force a snow and a microwave emission model to show that the use of a diurnal difference brightness temperature indicator is a valuable means for the investigation of melt onset in the study area. Finally, the new indicator is implemented in an algorithm that is used to derive the comprehensive data set "Melt Dynamics on Antarctic sea ice" [*Bareiss et al.*, 2007].

2. Data and Methods

[11] The investigations presented here are mainly based on long-term satellite data from active and passive microwave sensors. *DMSP Daily Polar Gridded Brightness Temperatures* [*Maslanik and Stroeve*, 2007] at 19 and 37 GHz for the period from 1987 to 2006 were used to analyze the general seasonal cycle of microwave T_B of Antarctic sea ice. Corresponding changes of σ^0 were determined from daily averages of the Ku-Band (13.4 GHz) QuikSCAT scatterometer [*Ezraty and Piolle*, 2001] between 1999 and 2006. *DMSP SSM/I Pathfinder EASE-Grid Brightness Temperatures* [*Armstrong et al.*, 2009], providing two T_B values per day with a time lag of approximately 12 hours, were acquired to increase the temporal resolution of the T_B monitoring. For the summer months of 2004/2005 (October to March), *DMSP F-13 swath data* with up to six T_B values per day were provided by the *U.S. Global Hydrological Resource Center* (GHRC). Sea-ice concentrations from 1978 to 2006 were derived from the *Bootstrap Sea Ice Concentrations* data set [*Comiso*, 2007], distributed by the *U.S. National Snow and Ice Data Center* (NSIDC).

[12] In-situ measurements of changes in snow properties were performed during the Ice Station POLarstern expedition between 28 November 2004 and 2 January 2005 in the western Weddell Sea (ISPOL [*Hellmer et al.*, 2006, 2008], Figure 1). ISPOL offered a unique opportunity to measure physical ice and snow properties with high temporal resolution during a 5-week drift station at the transition from spring to summer. The ISPOL floe was composed of patches of first- and second-year ice with mean snow thicknesses of 0.2 to 0.5 m and 0.75 m, respectively [*Haas et al.*, 2008; Nicolaus et al., submitted manuscript, 2009].

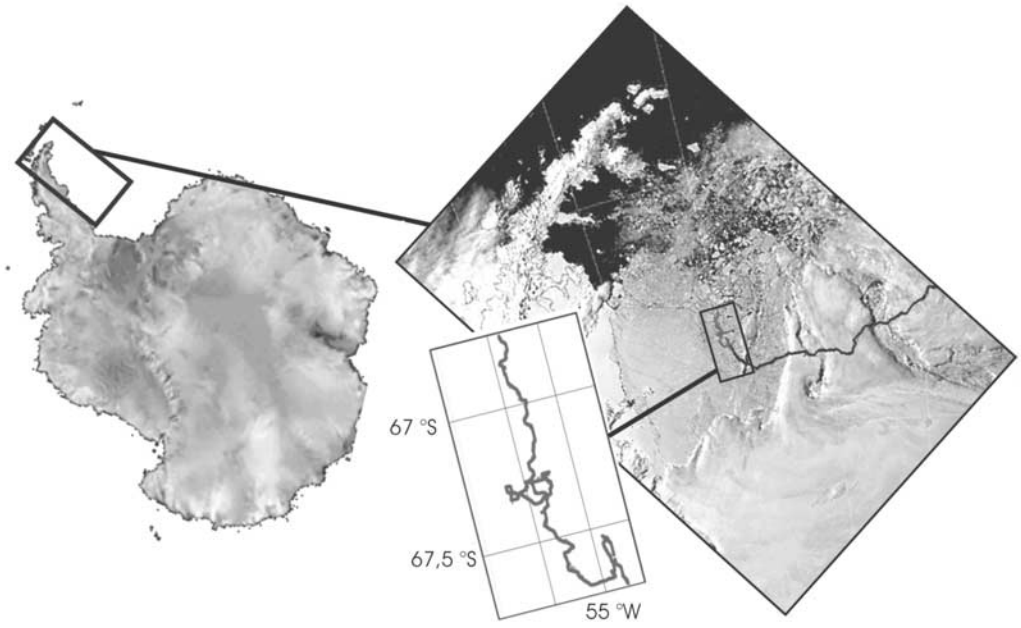

Figure 1. (left) Map of the Antarctic showing the ISPOL region (box) and (right) an AVHRR image (channel 2) of the western Weddell Sea from 25 December 2004. The course of *RV POLARSTERN* is marked by a gray line. (middle) The drift track is highlighted in the grid box.

[13] Several observational stations were established on the ISPOL floe to measure snow and ice properties and to determine their dependence on atmospheric boundary conditions by means of standard methods. The measurements included data from an Automatic Weather Station (AWS) that recorded wind speed, wind direction, air temperature (T_{air}), sea level pressure and relative humidity at 2 m as well as long-wave and short-wave radiation components. At each site, vertical profiles of snow wetness, snow density and snow temperature were measured at least daily (up to 6 times a day in the beginning of measurements). Surface temperature (T_{surf}) was calculated from the measured outgoing long-wave radiation, assuming an infrared emissivity of 1.0 for snow. In some cases, T_{surf} values larger than 0°C were obtained. Those are probably biased by radiative warming of the pyrgeometers and hence, they were skipped. More extensive information on the setup and details of the ISPOL field measurements is presented in *Willmes et al.* [2006] and Nicolaus et al. (submitted manuscript, 2009).

[14] In order to support interpretations of seasonal and diurnal variations of T_B, we used a *Microwave Emission Model for Layered Snowpacks* (MEMLS2 [*Wiesmann and Mätzler*, 1998]) to compute ε at 19 and 37 GHz for the snow pack in the ISPOL region. MEMLS2 is based on a six-flux radiative transfer model using a correlation-function approach to quantify snow structure, including multiple volume scattering by stratification and snow grains. The model utilizes empirical relationships between the scattering coefficient, microwave frequency and correlation length [*Wiesmann*, 1998] and computes ε in the frequency range from 5 to 100 GHz. MEMLS2 was forced with ISPOL measurements of snow temperature, density, wetness and grain size at any given layer such that one ε value per vertical profile is obtained.

[15] Two different data sets were used to compute ε. First, in-situ measurements of the required input parameters from all vertical snow profiles during ISPOL were divided into 50 layers through linear interpolation and subsequently combined into one input data set for MEMLS2. The only reason to choose 50 layers was that measurements from different sites with different snow heights and stratigraphies had to be interpolated into one data set in order to obtain input data with sufficient temporal resolution.

[16] Second, snow properties during ISPOL were computed with the one-dimensional mass- and energy-balance model SNTHERM [*Nicolaus*, 2006]. SNTHERM was initialized with snow properties as interpolated from measurements at different first-year ice sites in the beginning of ISPOL. This resulted in 23 layers of snow with a total height of 32 cm, differing in a combination of grain size, density and temperature [*Nicolaus*, 2006]. SNTHERM simulations were forced with ISPOL AWS measurements and the output was used to generate an alternative MEMLS2 input file with an improved temporal resolution of 5 minutes.

[17] Two principal melt onset indicators were calculated from T_B and tested against the seasonal cycles of sea-ice concentration and field observations at ISPOL. The *Horizontal Range* (HR)

$$\mathrm{HR} = \mathrm{T_B}19H - \mathrm{T_B}37H \tag{1}$$

[*Drobot and Anderson*, 2001a], as well as a modification of the *Cross-Polarized Gradient Ratio* (XPGR)

$$\mathrm{XPGR} = \mathrm{T_B}19H / \mathrm{T_B}37V \tag{2}$$

[*Abdalati and Steffen*, 1987] were calculated to detect events with significant snowmelt. While HR is expected to

Table 1. Frequency of Occurrence of DT_BA Differences Between Different SSM/I Sensors During Overlap Periods (F8–F11: December 1991; F11–F13: May 1995) for all Measurements and for Measurements With Ice Concentrations of >80%

DT_BA Difference (K)	<1	<2	<5	<10
	F08–F11			
All ($n = 1.525 \times 10^6$), frequency (%)	60.5	69.7	85.2	94.5
Sic > 80% ($n = 0.621 \times 10^6$), frequency (%)	95.6	96.6	97.9	98.8
	F11–F13			
All ($n = 1.525 \times 10^6$), frequency (%)	84	90.8	97.2	99.4
Sic > 80% ($n = 0.621 \times 10^6$), frequency (%)	90.5	95.4	99.1	99.9

approach zero when snowmelt begins, XPGR denotes snowmelt onset through exceeding a predefined threshold. Moreover, we extracted changes in sea-ice σ^0 from QuikSCAT data, where meltwater is expected to cause a significant temporary decrease [*Winebrenner et al.*, 1994; *Drinkwater and Liu*, 2000].

[18] The *Diurnal Brightness Temperature Amplitude* (DT_BA)

$$DT_BA = T_B\,\max - T_B\,\min \quad (3)$$

[*Willmes et al.*, 2006] was calculated by subtracting the smaller of the two diurnal T_B values (37 GHz vert. polarized) of the SSM/I Pathfinder data set ($T_B$min) from the larger T_B value ($T_B$max).

[19] During the observation period, three different SSM/I sensors (F8: October/1988–December/1991, F11: December/1991–March/1995 and F13: October/1995–March/2006) were used for the snow melt retrievals. As these radiometers have slightly different characteristics, it is necessary to intercalibrate their data sets. For daily T_B averages, sensor conversion methods were suggested by *Abdalati and Steffen* [1995] and *Stroeve et al.* [1998]. However, the SSM/I Pathfinder data used in this study include only T_B values from one ascending and descending orbit and thus no temporal averaging is performed. This, together with small intersensor differences between ascending and descending nodes, causes some apparent noise in the observed T_B. However, as DT_BA represents a 12-hour difference of raw T_B values, it is less sensitive to small shifts in the timing and absolute value of T_B measurements. During sensor overlap periods, DT_BA differences between sensors were on average less than 1 K in 68% of all measurements (<2 K for 80% of all measurements). If only areas with sea-ice concentrations of >80% were compared, DT_BA values between sensors agreed even better and differences were below 1 K on average for 93% and below 2 K for 96% of all measurements (Table 1). From this, we conclude that DT_BA can be used without intersensor conversion.

3. Results

[20] Weather and sea-ice conditions during ISPOL were characteristic of long-term conditions in the western Weddell Sea during early summer [*Willmes et al.*, 2006; *Bareiss and Goergen*, 2008]. Thus field and satellite data presented hereafter can be considered representative if some interannual variability is neglected.

3.1. Field and Satellite Data

[21] Figure 2 shows the evolution of meteorological parameters and snow properties, as well as of some microwave indicators during the drift station at the ship's position. The ISPOL period was dominated by long periods of overcast conditions and prevailing winds from north to east with a strength of 1 to 5 m s^{-1} [*Bareiss and Goergen*, 2008; Nicolaus et al., submitted manuscript, 2009]. T_{air} ranged between −5 and 0°C on the ISPOL floe and was slightly decreasing during December 2004. The influence of a high-pressure system in the southwestern Weddell Sea on 15 December caused the lowest average daily T_{air} of approximately −4.5°C in the drift period. Nicolaus et al. (submitted manuscript, 2009) show that incident short-wave radiation exceeded 900 W m^{-2} on clear-sky days, decreased to 0 W m^{-2} during every night and amounted to 400 to 600 W m^{-2} under overcast conditions. As a consequence net short-wave radiation averaged to 56 W m^{-2} over the whole observational period and was around 200 W m^{-2} during day time. Net heat flux was 8 W m^{-2} into the snow cover during ISPOL, consisting of 56 W m^{-2} net short-wave radiation, −34 W m^{-2} net long-wave radiation, and −14 W m^{-2} net turbulent heat fluxes. The energy input into the snow was equivalent to a potential snowmelt rate of 0.68 cm d^{-1}. However, less than 50% of the provided energy resulted in melting, but was rather consumed for warming the underlying sea ice [*Haas et al.*, 2008; Nicolaus et al., submitted manuscript, 2009].

[22] After 15 December, with decreasing SLP, T_{air} started to increase again. However, values of up to 0°C on daily average as measured in the beginning of December were not reached again. Because of floe breakups during storm events in the beginning and in the end of December the AWS had to be recovered and relocated, which caused gaps in the T_{air} and T_{surf} time series.

[23] The melt onset indicators XPGR and HR both were rising at the beginning of December (Figure 2b). This tendency ended in mid-December, when T_{air} was relatively low. However, XPGR and HR remained on a higher level as compared to the first half of the observation period. The daily average of T_B at 37 GHz (Figure 2c) was well aligned with the evolution of T_{air} (Figure 2a), showing an overall decrease during December. T_B from swath data, providing a higher temporal resolution, is characterized by a significantly increasing temporal variability which was mostly due to an increasing effect of the diurnal wetness cycle [*Willmes et al.*, 2006]. The observed daily averages of radar backscatter (σ^0, Figure 2d) evolve mostly opposite to T_B with a pronounced

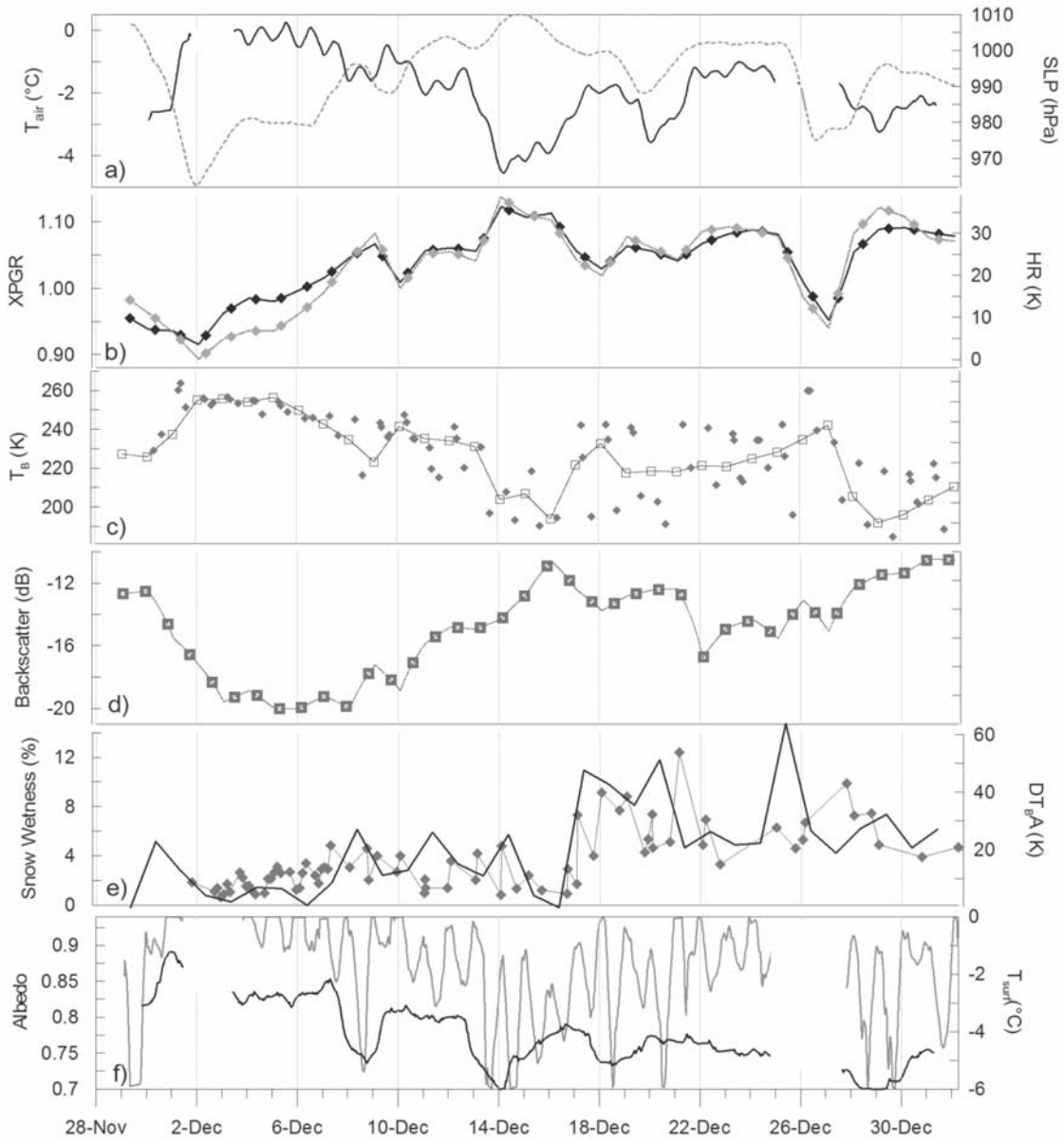

Figure 2. Meteorological conditions and snow and microwave properties during ISPOL field measurements from 28 November 2004 to 2 January 2005. (a) Moving averages of 2-m AWS air temperature T_{air} (5-min values, n = 289, solid line) and sea-level pressure at Polarstern's onboard meteorological station (dotted line); (b) XPGR (black) and HR parameters (gray) from daily T_B averages; (c) daily average T_B (line with white squares) and swath T_B (gray dots) at time of acquisition; (d) daily average of QuikSCAT Ku-band backscatter σ^0; (e) vertically averaged daytime snow wetness (line with dots) and DT_BA from SSM/I pathfinder data (black line); (f) moving averages of the albedo (black) and temperature (gray) of the snow surface (5-min values, n = 289). Plotted satellite data represent the pixel containing the ISPOL position at the respective date.

decrease in the beginning and a maximum in mid-December. As shown in Figure 2e, the amplification of the diurnal T_B cycle (DT_BA, black line) was accompanied by an increase of the vertically averaged daytime snow wetness with values reaching on average more than 5% after 15 December.

[24] Surface albedo, calculated as the ratio of reflected and incident short-wave radiation, declined from 0.9 to approximately 0.75, which was not enough to trigger significant snowmelt-albedo feedback processes (Nicolaus et al., submitted manuscript, 2009). At the surface, snow temperature was at 0°C in the first days of December (T_{surf}, Figure 2f). Afterwards, surface melting occurred only shortly around noon while the snow cooled down from the surface and refroze during nighttimes. Here, one has to differentiate between the interdiurnal and the diurnal cycles of freezing and rethawing. The first is driven by the influence of changing air masses and weather events and is superimposed to the T_{air} and radiatively driven diurnal cycle [*Vihma et al.*, 2009] of snow wetness. Significant

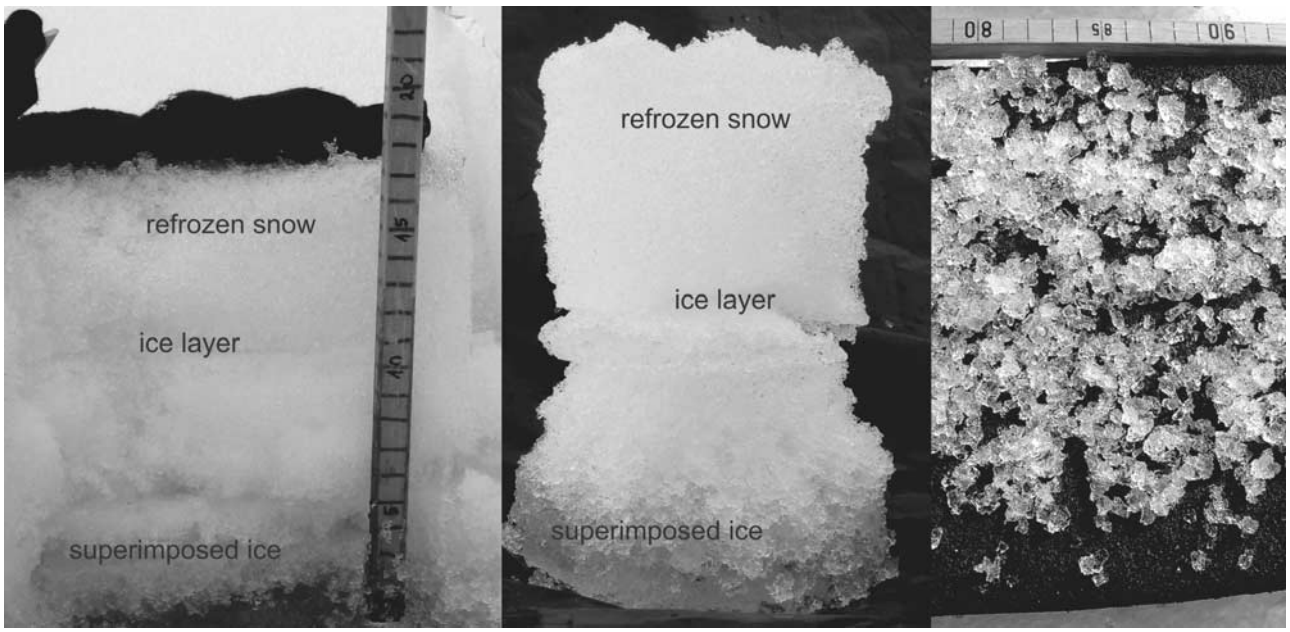

Figure 3. (left) Snow on first-year sea ice (FYI) with internal ice layer. (center) Refrozen snow with superimposed ice at the bottom, sample taken over FYI. (right) Rounded snow grains/melt clusters at the end of the field measurements.

weather events mostly weaken the diurnal cycle strength of snow wetness by causing either melt that is persistent throughout at least 24 hours (see warm air advection from 2 to 4 December) or through permanent freezing conditions (see influence of cold air during mid-December). Except from those weather events, we were observing pronounced diurnal cycles of freezing and rethawing. However, the 0°C isotherm never reached the snow-ice interface during the ISPOL period. Our field measurements indicate that the freeze-thaw cycles resulted in a growth of snow grains, the formation of internal ice layers and eventually, discontinuous superimposed ice (Figure 3) [*Haas et al.*, 2008; Nicolaus et al., submitted manuscript, 2009].

[25] As stated by *Willmes et al.* [2006] the summer of 2004/2005 did not show any pronounced snowmelt signals in T_B and σ^0 prior to or after ISPOL. Moreover, this summer was not special in this concern with regard to the long-term variability from 1994 to 2005.

[26] We conclude that the most convenient and reliable way to observe snowmelt patterns on Antarctic sea ice is a monitoring of the characteristic and pronounced diurnal freeze-thaw cycles rather than a sophisticated detection of rare events with strong melt. This is easily done using the diurnal difference brightness temperature indicator DT_BA. The weak and slow transition from dry to wet snow, together with the absence of persistent melting make conventional melt indicators as XPGR, HR or decreases of σ^0 unfeasible for melt studies in the Southern Ocean.

3.2. Freeze-Thaw Cycles, Microwave Emissivity and the DT_BA Melt Indicator

[27] The prevailing freeze-thaw melt pattern lends itself to be monitored in strength and variability through the DT_BA parameter. Here, we compute subdaily variations of ε at the ISPOL experimental sites with the MEMLS2 model with basically two intentions. First, to get a better insight into how changes of snow properties affect the microwave brightness temperature and second, to show that DT_BA is a valuable means for monitoring the succession of snowmelt in our study area.

[28] Figure 4 shows the modeled evolution of ε at 37 GHz with measured snow properties as input parameters (black diamonds). The modeled ε decreases slightly during the ISPOL drift. Unfortunately, the frequency of snow measurements was not high enough to fully capture the diurnal cycle throughout the entire drift period as measurements were performed only up to two times a day excluding nighttimes after 6 December. Hence no changes in the strength of the diurnal component can be assessed. The overall decrease of ε from approx. 0.6 to 0.4 is connected with increasing grain sizes. The simulations of ε at 19 and 37 GHz based on the outputs of the SNTHERM snow model provide a much higher temporal resolution (gray and black lines). SNTHERM captures subdaily variations of snow wetness and the accompanied structural changes of the snow pack. Thus strong diurnal ε cycles of up to 0.5 are found in the output of MEMLS2 after 30 November. The overall evolution of ε is strongly coupled with changes in T_{air}, showing an increase at the beginning of December, a local minimum in mid-December and a subsequent increase. Superimposed to this, we find a diurnal cycle of ε values, which gains intensity toward the end of the ISPOL drift. The period of relatively low T_{air} in mid-December is causing a small diurnal variability of ε and interrupts the overall evolution of the freeze-thaw-cycle strength. As the ε values modeled from field data do not decrease at the same time this might be due to an overestimation of the atmospheric forcing to the relevant snow properties within SNTHERM. In general, a decrease of ε during December is revealed from MEMLS2 results based on field data, whereas an increasing diurnal cycle is shown in MEMLS2 results from SNTHERM outputs.

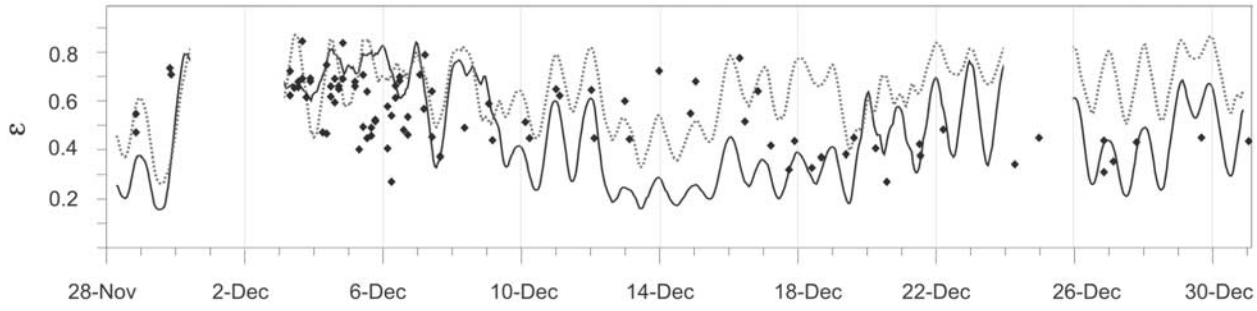

Figure 4. Microwave emissivity (ε) 37 GHz of the snow pack on the ISPOL drift floe, modelled with MEMLS2 from in-situ measurements (snow temperature, density, wetness, grain size) as averaged over all snow profiles (black diamonds) and ε at 19 GHz (grey line) and 37 GHz (black line) modelled with MEMLS2 from SNTHERM simulations of snow properties [*Nicolaus et al.*, 2006] with a temporal resolution of five minutes (AWS).

[29] The presented decrease and strong diurnal oscillations of ε connect the observed snow metamorphosis with mainly two microwave signatures. First, the typical decrease of daily averaged T_B during summer [*Willmes et al.*, 2006] and second, the enhanced diurnal T_B variability. The latter is also very evident in the time series of 37 GHz (vert. pol.) twice-daily SSM/I pathfinder data for the years of 1988 throughout 2006. As shown in Figure 5, the seasonal T_B cycle is clearly characterized by strong diurnal T_B cycles during the summer months with great regularity.

[30] These results suggest that the diurnal component of brightness temperature variations on Antarctic sea ice is most suitable to indicate the onset of summer conditions with large diurnal cycles of snow wetness. Daily averages of active and passive microwave data do not respond sufficiently to weak and temporally limited snowmelt for long-term investigations. A comparison of our field data with the evolution of different satellite parameters reveals that the diurnal T_B cycle provides the best proxy for the succession of melt. From this, we see the best potential to assess the large-scale and long-term summer melt characteristics on Antarctic sea ice from microwave satellite data in the DT_BA indicator. The seasonal DT_BA evolution with increasing values during early summer (Figure 2d) can be explained by the in-situ observed freeze-thaw cycles and is supported by the modeled emissivity variations of the snow pack (Figure 4). High DT_BA values indicate pronounced daytime snow wetting and overnight refreezing, while the longer-term daily average of T_B is slowly decreasing because of the associated and irreversible snow metamorphism.

[31] We use DT_BA with the explicit intention of detecting the *Early Melt* stage as this is found to be the dominating snowmelt feature in the ISPOL region and also in most sea-ice regions of the Southern Ocean except from the marginal ice zones [*Haas*, 2001; *Kern and Heygster*, 2001; *Drinkwater and Liu*, 2000]. Our method is not capable to resolve other melt processes that might contribute to the total sea-ice and surface decay. Those are mainly bottom and lateral melt of sea ice through heat supplied from the ocean.

3.3. Regional and Interannual Variability of Snowmelt Onset

[32] In order to detect the onset of typical summer snowmelt in the Southern Ocean, a DT_BA threshold algorithm (*Melt Detection Algorithm*, MeDeA) was defined. MeDeA detects the first date of a 5-day moving average of DT_BA exceeding a value of 10 K for at least three consecutive days (Figure 6). Threshold and moving window size were chosen to capture snow conditions as observed on the third day of measurements during the ISPOL drift (30 November 2004) when the snow surface started to become wet during the day and refroze during nighttimes (Figures 3e, 3d, and 6). A moving average of DT_BA was chosen in order to reduce the influence of singular events. MeDeA also queries sea-ice concentration data and discards pixels with an ice concentration of less than 80%.

[33] The comprehensive data set *Melt Dynamics on Antarctic Sea Ice* (MeDAntS) was generated by applying MeDeA to the full 18-year data set of SSM/I pathfinder data [*Bareiss et al.*, 2007]. The data set contains dates of snowmelt onset on Antarctic sea ice from October 1988 to March 2006 and is available online at the PANGAEA database (http://doi.pangaea.de/10.1594/PANGAEA.701389). Maps derived from MeDAntS show a high spatial and temporal variability of snowmelt onset (Figures 7a and 7b, and 8a).

[34] Meridional gradients with a delayed melt onset at higher latitudes can be found. The earliest snowmelt (beginning of October) occurs regularly in the northern Weddell, Amundsen and Ross Seas. East and West of the Antarctic Peninsula snowmelt is detected much more often than in the East Antarctic (Figure 8b). The standard deviation of melt onset dates in the observed period is shown in Figure 8c. In regions with frequent occurrences of snowmelt, the detected dates can have a standard deviation of up to 30 days with slightly larger values in the Amundsen Sea than in the Weddell Sea.

[35] There are large areas which are ice covered in the beginning of October (thin line in Figures 7a and 7b) but are not affected by surface melting as detected with MeDeA (white areas south of the ice edge). These areas are most often found in the eastern part of the Southern Ocean, in the marginal ice zones, in the southern Weddell Sea and in the Ross Sea. Here, the evolution of the snow and ice surface probably differs in three alternative ways from what we described above for the perennial ice in the ISPOL area: (1) surface melting might be much stronger than on the perennial ice without significant refreezing during nighttimes, (2) surface flooding (especially in the marginal ice zones) might dominate the T_B signal and mask out diurnal

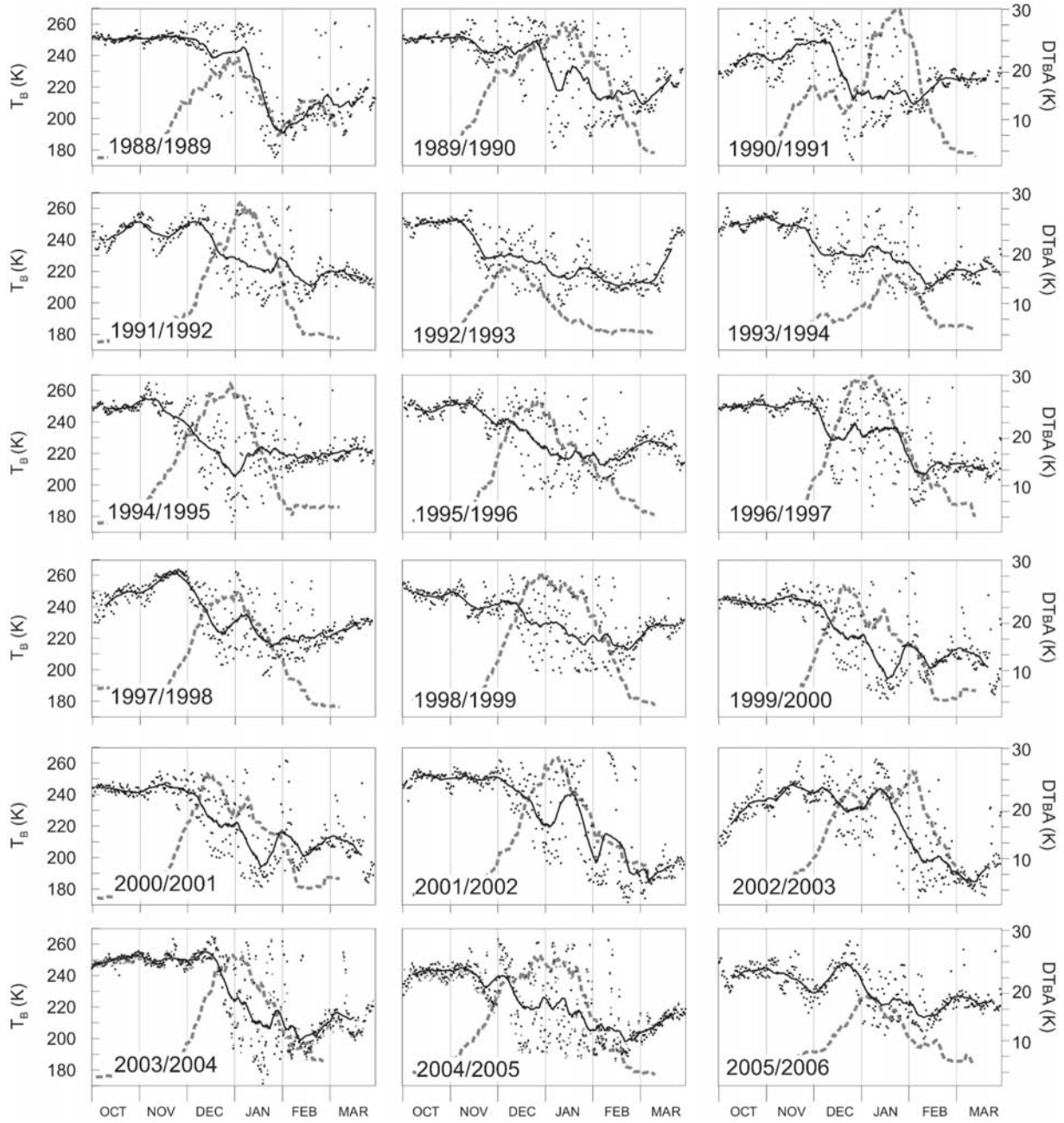

Figure 5. Evolution of SSM/I swath T_B at 37 GHz vert. polarized (dots), 15-days moving average (black line) and 5-days moving average of the derived DT_BA parameter (thick dotted line) at the ISPOL start position in the western Weddell Sea from October to March for the summers of 1988/1989 to 2005/2006.

cycles, or (3) the ice disintegrates, through breakup, lateral and basal melting before surface melting can take place. These effects, probably in combination with each other, are responsible for the white areas in the MeDeA melt onset maps. The proportion of melt areas (gray shaded) to "no surface melt detectable" areas (white) within the total sea-ice area shows a very high interannual variability.

4. Discussion

[36] *Livingstone et al.* [1987] separated snowmelt on sea ice in the Arctic into three different stages (*Early Melt, Melt Onset, Advanced Melt*) with the *Early Melt* stage being characterized through refreezing of the snow during night-times. *Harouche and Barber* [2001] found 4 characteristic clusters in the satellite data feature space of Arctic sea ice during summer. Our results suggest that fewer phenomenological stages of snowmelt are found on Antarctic sea ice compared to the Arctic.

[37] Freeze-thaw cycles are prevailing throughout the summer in the perennial Antarctic sea-ice zone, indicating that the *Early Melt* state according to *Livingstone et al.* [1987] is the most dominant snowmelt feature. The *Melt Onset* transition, as detected on Arctic sea ice [i.e.,

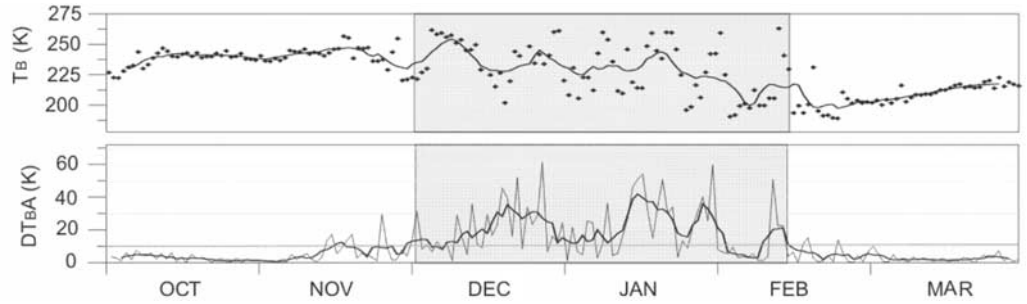

Figure 6. (top) Evolution of SSM/I pathfinder T_B at 37 GHz (dots) and 7-days moving average (black line) from October 2004 to March 2005 at the ISPOL area. (bottom) Daily DT_BA (gray line) and 5-days moving DT_BA average at the same position and time. The gray box highlights the summer melt period as detected with MeDeA; gray line indicates the 10-K threshold.

Anderson and Crane, 1994; *Anderson*, 1997; *Smith*, 1998; *Drobot and Anderson*, 2001a; *Belchansky et al.*, 2004a], however, is also found irregularly in the Antarctic but mostly limited to the marginal ice zones. Accordingly, our algorithm MeDeA does not detect melting in these regions because strong melt implies no refreezing and thus, induces low DT_BA values. Here, the approach of *Drinkwater and Liu* [2000] seems to be more suitable for melt detection

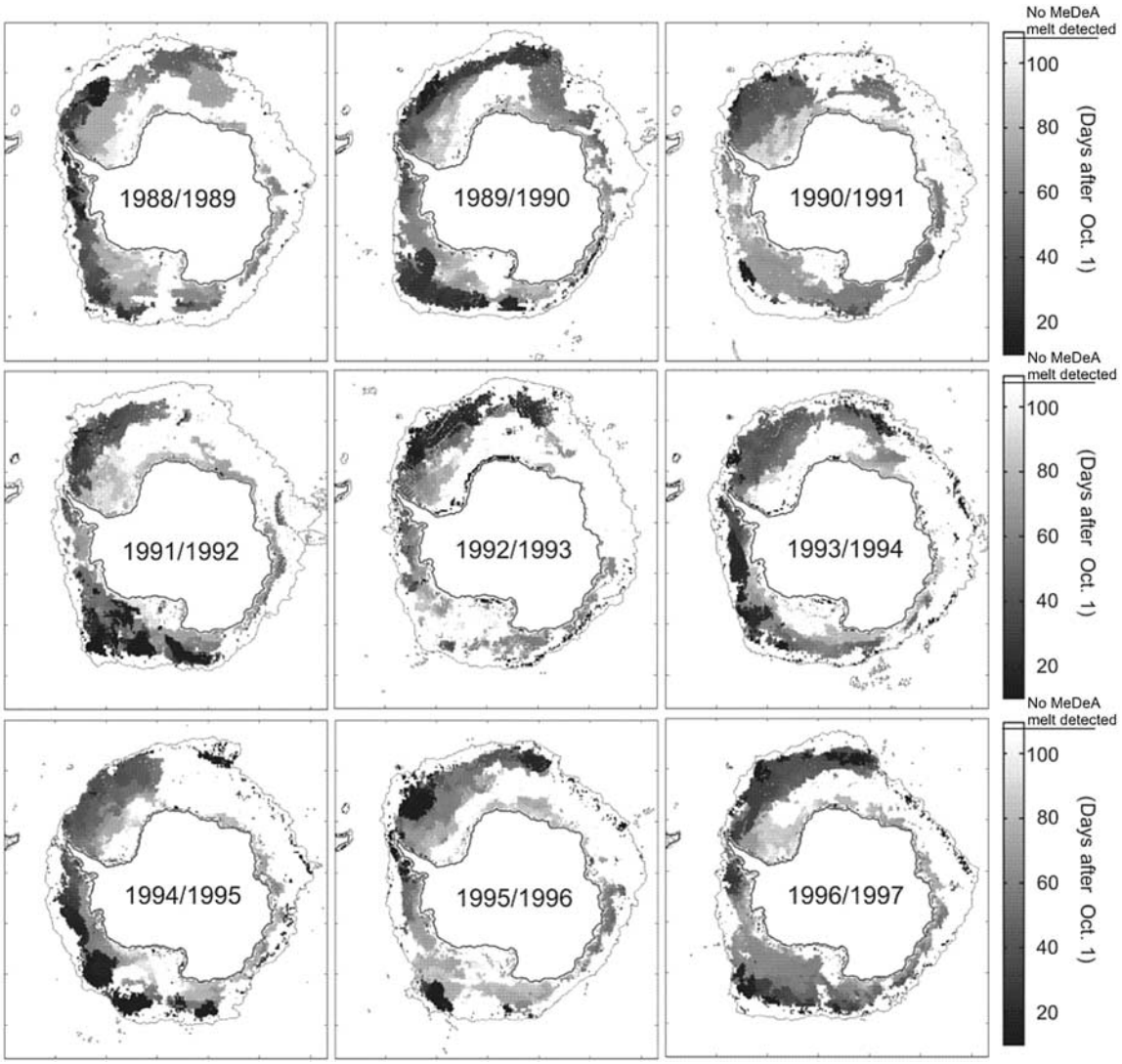

Figure 7a. Spatial variability of snowmelt onset in days after 1 October for the respective year on Antarctic sea ice as derived with MeDeA, 1988–1996; the thin line marks the ice edge on 1 October. White areas within the ice area denote sea ice where no surface melt is occurring according to MeDeA.

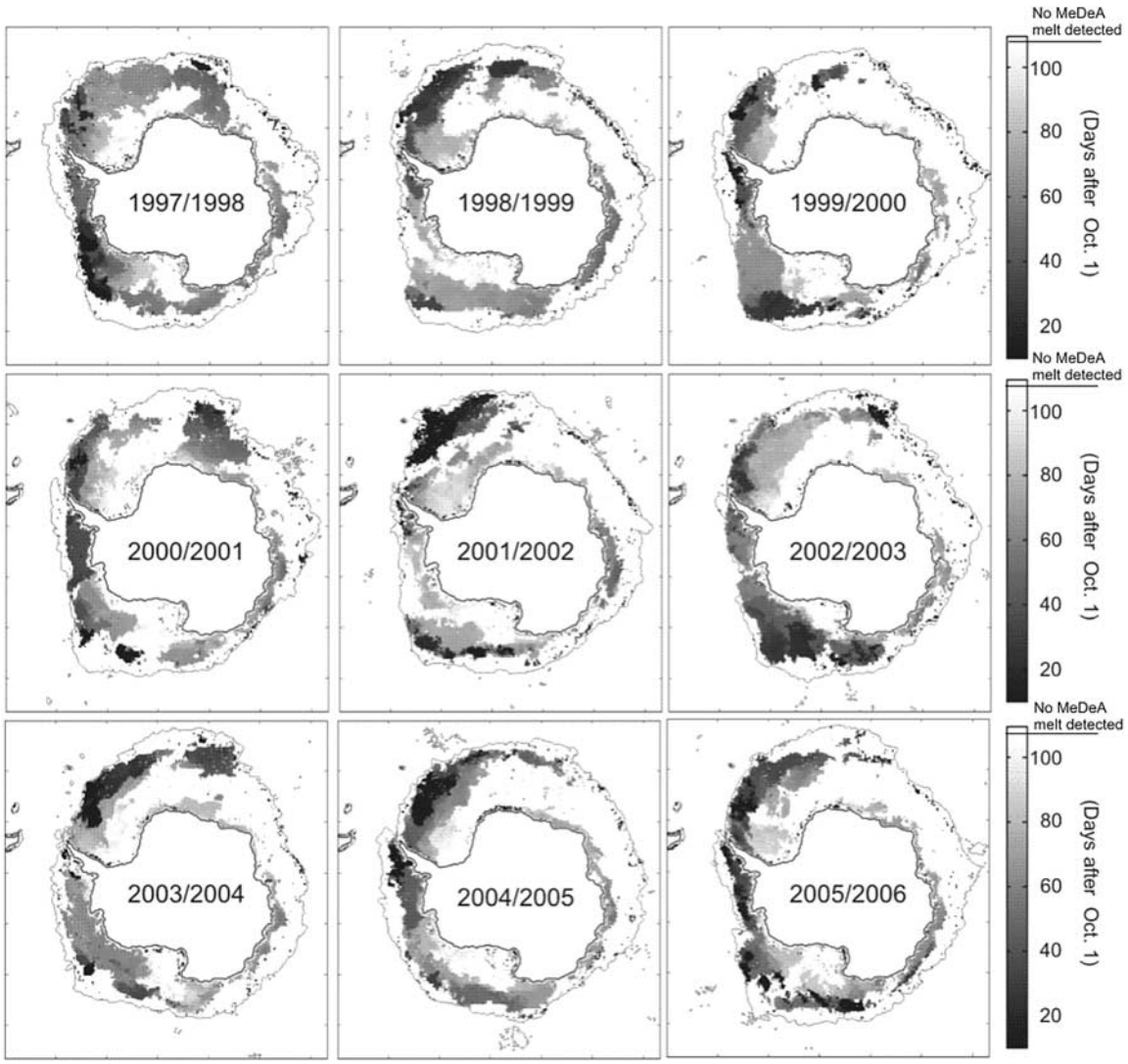

Figure 7b. Same as Figure 7a but for 1997–2006.

although it might be influenced by the widespread occurrence of snow wetting through flooding.

[38] Also south of the marginal ice zones, we found large areas where MeDeA indicates that no snowmelt occurs. This applies mainly to the southern Weddell and Ross Seas as well as to the entire Indian Ocean and Western Pacific sectors (Figure 8b) north of the coastal regions. A possible explanation is that the Weddell Sea south of 70° is located southward of the Antarctic Circumpolar Trough [*Simmonds and Keay*, 2000; *Turner and Pendlebury*, 2002] which

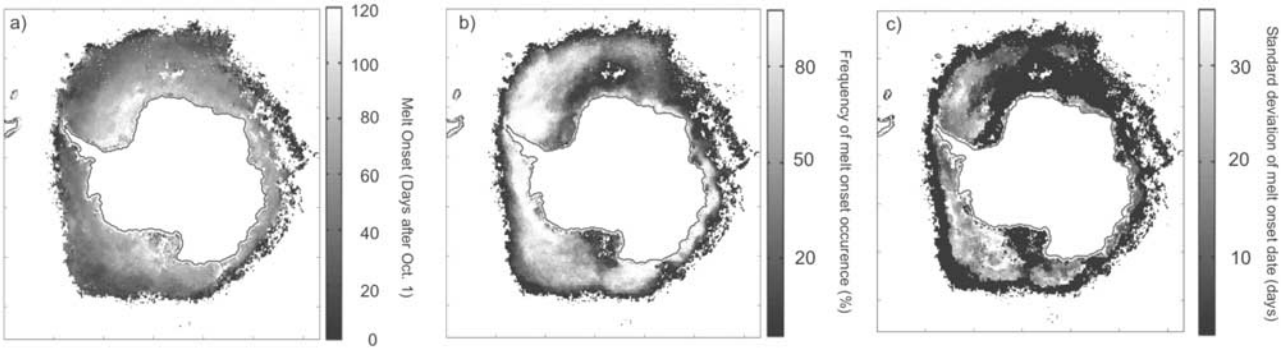

Figure 8. (a) Average date of snowmelt onset in days after 1 October on Antarctic sea ice, 1988–2006. (b) Spatial variability of the frequency of snowmelt occurrence, 1988–2006. (c) Standard deviation of melt onset date (days) with pixel providing less than 50% melt onset frequency marked as black.

diminishes the influence of warm air advection in this area. In the southern Ross Sea, low sea-ice concentrations due to the Ross Sea Polynya cause infrequent observations of snowmelt. In the Indian Ocean and Western Pacific sectors, sea-ice advects and disintegrates very fast once under the influence of the Antarctic Circumpolar Current. Thus bottom and lateral melt are dominating over surface melt in those areas.

[39] In contrast, east and west of the Antarctic Peninsula MeDeA snowmelt is very frequent, which probably results from increased perturbation of the general atmospheric flow and the entrainment of warm and moist air from lower latitudes.

[40] Melt detection is sensitive to the parameterization of MeDeA. A higher (lower) DT_BA threshold results in generally later (earlier) melt onset dates and a smaller (larger) total melt area. For example, an increase of the threshold from 10 K to 12.5 K results in a 20% reduction of the area where melt is detected. The largest changes occur in the marginal ice zones, where sea ice deteriorates very fast and thus, diurnal T_B cycles are found already early in summer but do not reach as large values as further south. Freeze onset dates were detected with MeDeA by using the above mentioned criteria and applying the DT_BA time series from October to March backward to each pixel. However, most often ice disintegrates through advection and basal melting before surface refreezing takes place, so that no freeze-up dates could be determined. The detection of snowmelt duration during summer is restricted to the perennial ice areas which are small in the Antarctic compared to the Arctic.

[41] In this study, field data were used to support the interpretation of large-scale satellite data. Although ice properties are spatially variable, we are confident that the observed processes can be extrapolated to large regions. No comparable data set of snow properties on Antarctic sea ice at the transition from spring to summer existed so far. The ISPOL floe in the western Weddell Sea was chosen to be representative of the surrounding area and measurements were performed on each aggregated ice type and characteristic snow depth as well as on remote floes visited by helicopter [*Hellmer et al.*, 2008; *Haas et al.*, 2008]. Moreover, ground data were collected along the transect from the ice edge to the ISPOL start position, improving our overview of the spatial and temporal variability of snow and ice properties.

[42] Our observations of strong snow metamorphism on Antarctic sea ice confirm earlier field investigations by *Massom et al.* [2001] and *Haas et al.* [2001]. Pronounced diurnal cycles of atmospheric conditions, mainly incident short-wave radiation are inducing temporal surface melt. However, in comparison to the Arctic, the air in our study area was colder, surface albedo higher and more energy from the snow was returned to the atmosphere via turbulent fluxes [*Vihma et al.*, 2009].

[43] Simulations of seasonal snow ablation in the Arctic and Antarctic by *Nicolaus et al.* [2006] as well as in-situ observations during early summer [*Vihma et al.*, 2009; Nicolaus et al., submitted manuscript, 2009] support the observation of strong hemispheric contrasts in the succession of snowmelt and the enhanced contribution of evaporation to snow mass losses in the Antarctic. As snow metamorphism dominates over snowmelt, the surface does not become opaque for microwave radiation. Therefore the microwave properties of the underlying sea ice influence the observed microwave signatures as well. However, using a diurnal T_B indicator instead of daily averages of T_B seems to provide a much better opportunity to observe processes in the upper snow layer.

[44] Snowmelt will be underestimated with increasing fractions of open water within one pixel because DT_BA is approximately zero for open water. The T_B signal observed from space is generated in a vertical layer that is variable in thickness, depending mainly on snow wetness, density, grain characteristics and structural inhomogenities. The vertical temperature profile and the position of the 0°C isotherm in the snow might influence the strength of the diurnal T_B amplitude.

[45] The DT_BA parameter was chosen to indicate snowmelt processes. This parameter does not necessarily capture the maximum amplitude of T_B during one day as satellite swaths are unequally distributed in time. However, DSMP satellites are sun synchronous and scanning at fixed local times with each swath. Hence they are capable of providing representative temporal changes of the diurnal amplitudes from twice-daily T_B values. In general, increasing the temporal resolution of observations of snow properties with sea-ice modeling might significantly increase the accuracy of the projected seasonal evolution of the ice cover [*Hanesiak et al.*, 1999].

5. Conclusions and Outlook

[46] Long-term microwave satellite data were examined in combination with field data from a drift station in the Weddell Sea during summer 2004/2005 to investigate snowmelt processes on Antarctic sea ice as well as their interannual and spatial variability.

[47] According to our measurements, diurnal freeze-thaw cycles are prevailing throughout the summer on perennial Antarctic sea ice. The absence of strong and persistent snowmelt impedes a transfer of melt detection methods from the Arctic. Field measurements and a microwave emission model reveal that the diurnal T_B cycle provides the best proxy for the succession of melt. Thus we suggest a new approach that accounts for the hemispheric peculiarities of the snowmelt period, in particular the diurnal component of snow wetness.

[48] Our study provides new insight into the characteristics of the Antarctic snow/sea-ice surface during summer and introduces a method to identify the *Early Melt* Stage from long-term microwave satellite data. According to our findings, the DT_BA indicator can be used in a threshold algorithm to detect the timing of the onset of snowmelt on Antarctic sea ice.

[49] We have applied our algorithm to the available 18-year long SSM/I record to prepare the data set MeDAntS [*Bareiss et al.*, 2007], which integrates snowmelt onset dates on Antarctic sea ice for the period from 1988 to 2006 and can be updated each year. We will use the MeDAntS melt product for climate studies relating the occurrence of melt signals to variations of meteorological boundary conditions, and for the detection of possible trends in snowmelt patterns with regards to other changing climate signals.

[50] We are planning on preparing a comparative data set *Melt Dynamics on Arctic Sea ice* (MeDArcS) to assess the contribution of freeze-thaw cycles and thus, the Early Melt Stage, to the overall evolution of the seasonal snow and sea-ice decay in the Arctic. Further investigations of the presented data might explore the sum of diurnal T_B differences accumulated over a certain period in order to assess the total freeze-thaw rates rather than melt onset dates. An advanced algorithm, combining a diurnal approach with conventional melt detection, might be useful in preparing climatologies of snowmelt patterns and superimposed-ice formation estimations for sea ice in both hemispheres.

[51] **Acknowledgments.** The authors are very grateful to C. Mätzler for providing the model MEMLS2. Moreover we would like to thank the ISPOL field party for technical support and encouraging discussions. SSM/I brightness temperatures and sea-ice concentration data were kindly provided by the U.S. National Snow and Ice Data Center (NSIDC), University of Colorado, Boulder; SSM/I swath data by the NASA Global Hydrology Resource Center (GHRC); and active microwave satellite data (ERS, QuikSCAT) by the French Institute for Marine Research (IFREMER). This study was funded by the German Research Foundation (DFG) under contracts HA2724/4-1 and BA2060/2-1.

References

Abdalati, W., and K. Steffen (1987), Snowmelt on the Greenland ice sheet as derived from passive microwave satellite data, *J. Clim.*, *10*(2), 165–175.

Abdalati, W., and K. Steffen (1995), Passive microwave-derived snow melt regions on the Greenland ice sheet, *Geophys. Res. Lett.*, *22*(7), 787–790.

Anderson, M. R. (1987), The onset of spring melt in first-year ice regions of the Arctic as determined from scanning multichannel microwave radiometer data for 1979 and 1980, *J. Geophys. Res.*, *92*(C12), 13,153–13,163.

Anderson, M. R. (1997), Determination of a melt onset date for Arctic sea ice regions using passive microwave data, *Ann. Glaciol.*, *25*, 382–387.

Anderson, M., and R. Crane (1994), Springtime microwave emissivity changes in the southern Kara Sea, *J. Geophys. Res.*, *99*(C7), 14,303–14,309.

Anderson, M. R., and S. D. Drobot (2001), Spatial and temporal variability in snowmelt onset over arctic sea ice, *Ann. Glaciol.*, *33*, 74–78.

Andreas, E. L., and S. F. Ackley (1982), On the differences in ablation seasons of Arctic and Antarctic sea ice, *J. Atmos. Sci.*, *389*, 440–447.

Ashcraft, I. S., and D. G. Long (2005), Differentiation between melt and freeze stages of the melt cycle using SSM/I channel ratios, *IEEE Trans. Geosci. Remote Sens.*, *43*(6), 1317–1323.

Armstrong, R. L., K. W. Knowles, M. J. Brodzik, and M. A. Hardman (2009), DMSP SSM/I Pathfinder daily EASE-Grid brightness temperatures, 1988–2006, Digital media, Natl. Snow Ice Data Cent., Boulder, Colo.

Barber, D. G., A. K. Fung, T. C. Grenfell, S. V. Nghiem, R. G. Onstott, V. I. Lytle, D. K. Perovich, and A. J. Gow (1998), The role of snow on microwave emission and scattering over first-year sea ice, *IEEE Trans. Geosci. Remote Sens.*, *36*(5), 1750–1763.

Bareiss, J., and K. Goergen (2008), ISPOL weather conditions in the context of long-term climate variability in the northwestern Weddell Sea, *Deep Sea Res. Part II*, *55*(8), 918–932, doi:10.1016/j.dsr2.2007.12.017.

Bareiss, J., S. Willmes, and C. Haas (2007), New data set of onset of annual snowmelt on Antarctic sea ice, *Eos Trans. AGU*, *88*(22), 237–241.

Belchansky, G., D. C. Douglas, I. Mordvintsev, and N. Platonov (2004a), Estimating the time of melt onset and freeze onset over Arctic sea ice area using active and passive microwave data, *Remote Sens. Environ.*, *92*, 21–39.

Belchansky, G. I., D. C. Douglas, and N. G. Platonov (2004b), Duration of the Arctic sea ice melt season: regional and interannual variability, 1979–2001, *J. Clim.*, *17*, 67–80.

Comiso, J. C. (1983), Sea ice effective microwave emissivities from satellite passive microwave and infrared observations, *J. Geophys. Res.*, *88*(C12), 7686–7704.

Comiso, J. (2007), Bootstrap sea ice concentrations from NIMBUS-7 SMMR and DMSP SSM/I, 1988–2006, Digital media, Natl. Snow Ice Data Cent., Boulder, Colo.

Comiso, J. C., T. C. Grenfell, M. Lange, A. W. Lohanick, R. K. Moore, and P. Wadhams (1992), Microwave remote sensing of the southern ocean ice cover, in *Microwave Remote Sensing of Sea Ice*, *Geophys. Monogr. Ser.*, vol. 68, edited by F. D. Carsey, pp. 243–259, AGU, Washington, D. C.

Curry, J. A., J. L. Schramm, and E. E. Ebert (1995), Sea-ice albedo climate feedback mechanism, *J. Clim.*, *8*(2), 240–247.

Drinkwater, M. R., and X. Liu (2000), Seasonal to interannual variability in Antarctic sea-ice surface melt, *IEEE Trans. Geosci. Remote Sens.*, *38*, 1827–1839.

Drobot, S. D., and M. R. Anderson (2001a), Comparison of interannual snowmelt-onset dates with atmospheric conditions, *Ann. Glaciol.*, *33*, 79–84.

Drobot, S. D., and M. R. Anderson (2001b), An improved method for determining snowmelt onset dates over Arctic sea ice using SMMR and SSM/I data, *J. Geophys. Res.*, *106*(D20), 24,033–24,049.

Eicken, H. (1998), Factors determining microstructure, salinity and stable-isotope composition of Antarctic sea ice: Deriving modes and rates of ice growth in the Weddell Sea, in *Antarctic Sea Ice Physical Processes, Interactions and Variability*, *Antarct. Res. Ser.*, vol. 74, edited by M. O. Jeffries, pp. 89–122, AGU, Washington, D. C.

Ezraty, R., and J. F. Piolle (2001), SeaWinds on QuickSCAT polar sea ice grids, *User Manual*, *CONVECTION Rep. 5*, 29 pp., Eur. Comm., Brussels, Belgium.

Fetterer, F., and N. Untersteiner (1998), Observations of melt ponds on Arctic sea ice, *J. Geophys. Res.*, *103*(C11), 24,821–24,836.

Haas, C. (2001), The seasonal cycle of ERS scatterometer signatures over perennial Antarctic sea ice and associated surface ice properties and processes, *Ann. Glaciol.*, *33*, 69–73.

Haas, C., D. N. Thomas, and J. Bareiss (2001), Surface properties and processes of perennial Antarctic sea ice in summer, *J. Glaciol.*, *47*(159), 613–625.

Haas, C., M. Nicolaus, S. Willmes, A. Worby, and D. Flinspach (2008), Sea ice and snow thickness and physical properties of an ice floe in the western Weddell Sea and their changes during spring warming, *Deep Sea Res. Part II*, *55*(8), 963–974, doi:10.1016/j.dsr2.2007.12.020.

Hanesiak, J. M., D. G. Barber, and G. M. Flato (1999), Role of diurnal processes in the seasonal evolution of sea ice and its snow cover, *J. Geophys. Res.*, *104*(C6), 13,593–13,603.

Harouche, I. P. F., and D. G. Barber (2001), Seasonal characterization of microwave emissions from snow-covered first-year sea ice, *Hydrol. Processes*, *15*, 3571–3583.

Hellmer, H. H., C. Haas, G. S. Dieckmann, and M. Schröder (2006), Sea ice feedbacks observed in western Weddell Sea, *Eos Trans. AGU*, *87*(18), 173–184.

Hellmer, H. H., M. Schröder, C. Haas, G. S. Dieckmann, and M. Spindler (2008), The ISPOL drift experiment, *Deep Sea Res. Part II*, *55*, 913–917.

Jeffries, M. O., A. P. Worby, K. Morris, and W. F. Weeks (1997), Seasonal variations in the properties and structural composition of sea ice and snow cover in the Bellingshausen and Amundsen Seas, *J. Glaciol.*, *43*(143), 138–151.

Kern, S., and G. Heygster (2001), Sea-ice concentration retrieval in the Antarctic based on the SSM/I 85.5 GHz polarization, *Ann. Glaciol.*, *33*, 109–114.

Koskinen, J. T., J. T. Pulliainen, and M. T. Hallikainen (1997), The use of ERS-1 SAR data in snow melt monitoring, *IEEE Trans. Geosci. Remote Sens.*, *35*(3), 601–610.

Lange, M. A., S. F. Ackley, P. Wadhams, G. S. Dieckmann, and H. Eicken (1989), Development of sea ice in the Weddell Sea, Antarctica, *Ann. Glaciol.*, *12*, 92–96.

Livingstone, C. E., R. G. Onstott, L. D. Arsenault, A. L. Gray, and K. P. Singh (1987), Microwave sea-ice signatures near the onset of melt, *IEEE Trans. Geosci. Remote Sens.*, *25*(2), 174–187.

Markus, T., and D. J. Cavalieri (2007), Interannual and regional variability of Southern Ocean snow on sea ice, *Ann. Glaciol.*, *44*, 53–57.

Maslanik, J., and J. Stroeve (2007), DMSP SSM/I daily polar gridded brightness temperatures, 1988–2006, Digital media, Natl. Snow Ice Data Cent., Boulder, Colo.

Maslanik, J. A., and R. G. Barry (1989), Short-term interactions between atmospheric synoptic conditions and sea-ice behaviour in the Arctic, *Ann. Glaciol.*, *12*, 113–117.

Massom, R., et al. (2001), Snow on Antarctic sea ice, *Rev. Geophys.*, *39*(3), 413–445.

Mote, T. L. (2007), Greenland surface melt trends 1973–2007: Evidence of a large increase in 2007, *Geophys. Res. Lett.*, *34*, L22507, doi:10.1029/2007GL031976.

Mote, T. L., and M. R. Anderson (1995), Variations in melt on the Greenland ice sheet based on passive microwave measurements, *J. Glaciol.*, *41*, 51–60.

Nicolaus, M. (2006), Beobachtung und Modellierung der Schneeschmelze und Aufeisbildung auf arktischem und antarktischem Meereis, Ph.D. thesis, Dept. of Geosciences, Univ. of Bremen, Germany.

Nicolaus, M., C. Haas, and J. Bareiss (2003), Observations of superimposed ice formation at melt-onset on fast ice on Kongsfjorden, Svalbard, *Phys. Chem. Earth*, *28*, 1241–1248.

Nicolaus, M., C. Haas, J. Bareiss, and S. Willmes (2006), A model study of differences of snow thinning on Arctic and Antarctic first-year sea ice during spring and summer, *Ann. Glaciol.*, *44*, 147–153.

Perovich, D. K. (1996), The optical properties of sea ice, *CRREL Monogr.*, *96*(1), 25 pp.

Perovich, D. K., S. V. Nghiem, T. Markus, and A. Schweiger (2007), Seasonal evolution and interannual variability of thew local solar energy absorbed by the Arctic sea ice-ocean system, *J. Geophys. Res.*, *112*(C3), C03005, doi:10.1029/2006JC003558.

Serreze, M. C., J. A. Maslanik, G. P. Scharfen, R. G. Barry, and D. A. Robinson (1993), Interannual variations in snow melt over Arctic sea ice and relationships to atmospheric forcings, *Ann. Glaciol.*, *17*, 327–331.

Simmonds, I., and K. Keay (2000), Mean southern hemisphere extratropical cyclone behaviour in the 40-year NCEP/NCAR reanalysis, *J. Clim.*, *13*(2), 873–885.

Smith, D. (1998), Observation of perennial Arctic sea ice melt and freeze-up using passing microwave data, *J. Geophys. Res.*, *103*(C12), 27,753–27,769.

Stroeve, J., L. Xiaoming, and J. Maslanik (1998), An intercomparison of DMSP F11- and F13-derived sea ice products, *Remote Sens. Environ.*, *64*, 132–152.

Tedesco, M. (2007), Snowmelt detection over the Greenland ice sheet from SSM/I brightness temperature daily variations, *Geophys. Res. Lett.*, *34*, L02504, doi:10.1029/2006GL028466.

Tucker, W. B., A. J. Gow, and W. F. Weeks (1987), Physical properties of summer sea ice in Fram Strait, *J. Geophys. Res.*, *92*(C7), 6787–6803.

Turner, J., and S. Pendlebury (Eds.) (2002), *The International Antarctic Weather Forecasting Handbook*, Bureau of Meteorology, Australian Government, Australia.

Vihma, T., M. M. Johansson, and J. Launiainen (2009), Radiative and turbulent surface heat fluxes over Antarctic sea ice in early summer, *J. Geophys. Res.*, doi:10.1029/2008JC004995, in press.

Wadhams, P. (2000), *Ice in the Ocean*, Gordon and Breach, New York.

Warren, S., I. G. Rigor, N. Untersteiner, V. F. Radionov, N. N. Bryazgin, Y. I. Aleksandrov, and R. Colony (1999), Snow depth on Arctic sea ice, *J. Clim.*, *12*(6), 1814–1829.

Wiesmann, A. (1998), Radiometric and structural measurements of snow samples, *Radio Sci.*, *33*(2), 273–289.

Wiesmann, A., and C. Mätzler (1998), Documentation for MEMLS 98.2, Microwave Emission Model of Layered Snowpacks, *Tech. Rep., Res. Rep. 98-2*, Microwave Dept., Inst. of Appl. Phys., Univ. of Bern, Switzerland.

Willmes, S., J. Bareiss, C. Haas, and M. Nicolaus (2006), The importance of diurnal processes for the seasonal cycle of sea-ice microwave brightness temperature during early summer in the Weddell Sea, *Ann. Glaciol.*, *44*, 297–302.

Winebrenner, D. P., E. D. Nelson, R. Colony, and R. D. West (1994), Observation of melt onset on multiyear arctic sea ice using ERS 1 synthetic aperture radar, *J. Geophys. Res.*, *99*(C11), 22,425–22,441.

J. Bareiss and S. Willmes, Department of Environmental Meteorology, University of Trier, Behringstr. 21, D-54286 Trier, Germany. (willmes@uni-trier.de)

C. Haas, Department of Earth and Atmospheric Sciences, University of Alberta, 1-26 Earth Sciences Building (Office Tory 2-105C), Edmonton, AB T6G 2E3, Canada.

M. Nicolaus, Polar Environmental Centre, Norwegian Polar Institute, N-9296 Tromsø, Norway.